

Fluid structure interaction

Andreas Strøm Slyngstad

01 01 01

Contents

1	Time discretization and optimization	3
1.1	Implementation of a one-step θ scheme	4
1.1.1	Temporal stability	5

Chapter 1

Numerical Results

In this chapter the numerical results for this thesis will be presented. The first and second chapters concern the verification and validation of the *One-step θ* scheme respectively. In the third and final chapter, different speed-up strategies are presented and compared

1.1 Verification

1.2 Validation of a One-step θ scheme

The numerical benchmark presented in [1] has been chosen for validation of the *One-step θ* scheme presented in chapter. The benchmark has been widely accepted throughout the fluid-structure interaction community as a rigid validation benchmark. This is mainly due to the diversity of tests included, challenging all the main components of a fluid-structure interaction scheme.

The computational domain is based on the *von Kármán vortex street* se (cite), where a cylinder is intentionally placed off center in a pipe. This configuration initiates a periodic shedding of vortices, as some fluid moves past the cylinder. In [1], an elastic flag is placed behind the cylinder.

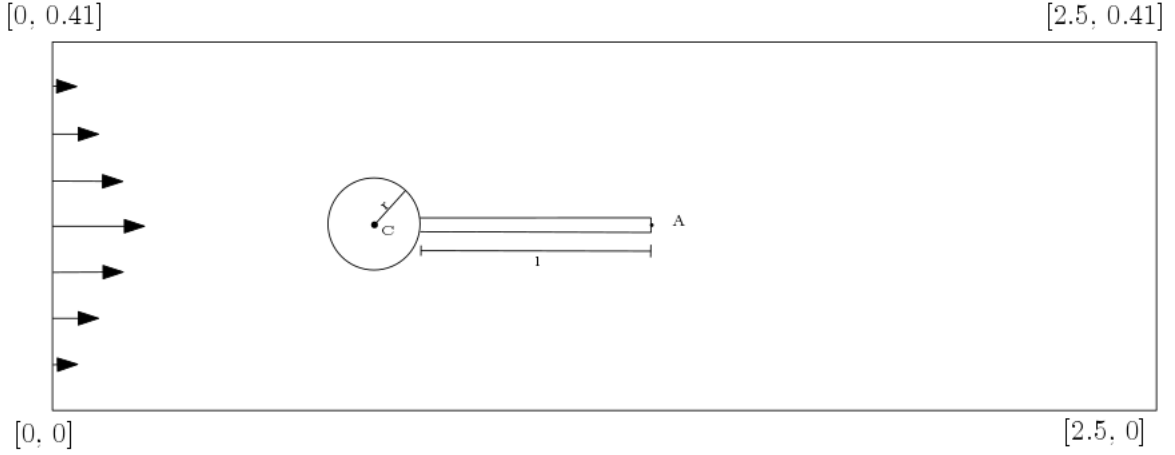


Figure 1.1: Computational domain of the validation benchmark

The benchmark is divided into three main test environments. In the first environment the fluid solver is tested for a series of different flow profiles.

The second environment regards the structure implementation, regarding bending of the elastic flag. The third environment the full fluid-structure interaction problem. The test environments are further divided into three different problems with increasing difficulty, posing different challenges to the implementation.

Several quantities for comparison are presented in [1] for validation purposes. The evaluation of these quantities are considered for fully developed flow,

- The position (x,y) of point $A(t)$ as the elastic flag undergoes deformation.
- Drag and lift forces exerted on of the whole interior geometry in contact with the fluid, consisting of the rigid circle and the elastic beam.

$$(F_D, F_L) = \int_{\Gamma} \sigma \cdot \mathbf{n} dS$$

The following environments and their sub-problems presents both steady state and periodic solutions. For the steady state solutions, the quantity of interest will be calculated for the last timestep. For the periodic solutions, the amplitude and mean values for the time dependent quantity are calculated from the last period of oscillations. The mean value and amplitude is given by,

$$\begin{aligned} \text{mean} &= \frac{1}{2} \max + \min \\ \text{amplitude} &= \frac{1}{2} \max - \min \end{aligned}$$

from the maximum and minimum value of the quantity of interest from the last period.

In [1], all steady state solutions seems to be calculated by solving a steady state equation such as the stokes equation for the fluid problem. The assumption is based on simulation parameters regarding time-step are only reported for the periodic

solutions. In this thesis all problems in [1], will be calculated by time integration. The main motivation is based upon that any given numerical errors regarding time integration will be intercepted at an earlier stage for a simpler problem. Therefore, the choice of timestep is chosen such that reasonable accuracy of the reference solution is attained.

In [1], details such as finite-element spaces and newton iteration criteria are not reported. Therefore, the following numerical results have been a process of trial and error. In the following section, an overview of each environment together with the numerical results will be presented. A formal discussion of the results are given at the end of each simulation environment. For each table, the error of the finest spatial and temporal refinement compared to the reference solution is reported .

Since the first two simulation environments are presented mainly in support of the third and final environment, they were not reported in OTHER CITE. Therefore results in the first two subsections will be compared with [1], while the third will consider both [1] and OTHER CITE.

1.2.1 Validation of fluid solver

The first test environment concerns the fluid dynamics part of the total FSI problem, to ensure the solver can handle flows in low Reynold-numbers regime. Two approaches for the validation are given in [1]. The first approach considers setup as a fluid-structure interaction problem, by setting the elastic flag close to rigid by manipulation of the structure paramters. Second, the flag can be set fully rigid and considered a purly flow problem. Hence, the fluid variation formulation can be reduced to

Find $\hat{\mathbf{v}}_f, \hat{p}_f$ such that

$$\begin{aligned} \left(\frac{\partial \hat{\mathbf{v}}}{\partial t}, \hat{\boldsymbol{\psi}}^u\right)_{\hat{\Omega}_f} + ((\hat{\mathbf{v}} \cdot \hat{\nabla})\hat{\mathbf{v}}, \hat{\boldsymbol{\psi}}^u)_{\hat{\Omega}_f} - (\hat{\sigma}, \hat{\nabla} \hat{\boldsymbol{\psi}}^u)_{\hat{\Omega}_f} - (\rho_f \mathbf{f}_f, \hat{\boldsymbol{\psi}}^u)_{\hat{\Omega}_f} &= 0 \\ (\nabla \cdot \hat{\mathbf{v}}), \hat{\boldsymbol{\psi}}^p)_{\hat{\Omega}_f} &= 0 \end{aligned}$$

The latter approach is chosen for this thesis, as only the variational formulation for the fluid is tested and removes any influence of the strucutre and mesh extrapolation discretization. Since $\hat{\Omega}_f = \Omega_f(t) \ t \in T$, the mesh velocity of the fluid $\frac{\partial \mathbf{T}_W}{\partial t} = 0$ and no deformation of the fluid domain is present.

The validation of the fluid solver is divided into the three sub-cases CFD1, CFD2 and CFD3. While CFD1 and CFD2 yields steady state solutions, CFD3 is a periodic solution.

Table 1.1: Benchmark environment

Fluid parameters			
parameter	CFD 1	CFD 2	CFD 3
$\rho^f [10^3 \frac{kg}{m^3}]$	1	1	1
$\nu^f [10^{-3} \frac{m^2}{s}]$	1	1	1
U	0.2	1	2
Re	20	100	200

A parabolic velocity profile on the form,

$$v_f(0, y) = 1.5U \frac{(H - y)y}{(\frac{H}{2})^2}$$

is set on the left channel inflow. H is the height of the channel, while the parameter U is set differently to each problem to induce different flow profiles.

At the right channel outflow, the pressure is set to $p = 0$. No-slip boundary conditions for the fluid are enforced on the channel walls, and on the inner geometry consisting of the circle and the elastic flag. The validation is based on the evaluation of drag and lift forces on the inner geometry for each sub-case. with comparison to [1]. Each sub-case will be conducted on four different mesh, with increasing refinement. The following tables presents the numerical results for each sub-case.

Table 1.2: CFD 1 Results

$\Delta t = 0.1 \quad \theta = 1.0$			
nel	ndof	Drag	Lift
1438	6881	13.60	1.089
2899	13648	14.05	1.126
7501	34657	14.17	1.109
19365	88520	14.20	1.119
Reference		14.29	1.119
Error		0.006 %	0.00 %

Table 1.3: CFD-2

$\Delta t = 0.01 \quad \theta = 1.0$			
nel	ndof	Drag	Lift
1438	6881 (P2-P1)	126.0	8.62
2899	13648 (P2-P1)	131.8	10.89
7501	34657 (P2-P1)	135.1	10.48
19365	88520(P2-P1)	135.7	10.55
Reference		136.7	10.53
Error		0.007 %	0.001 %

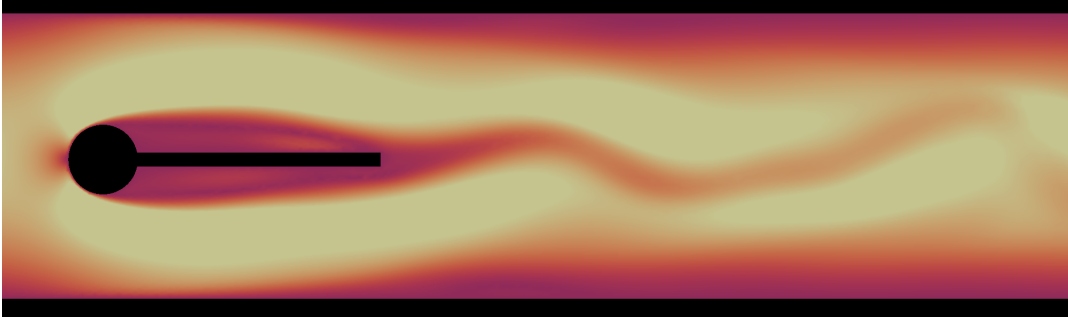
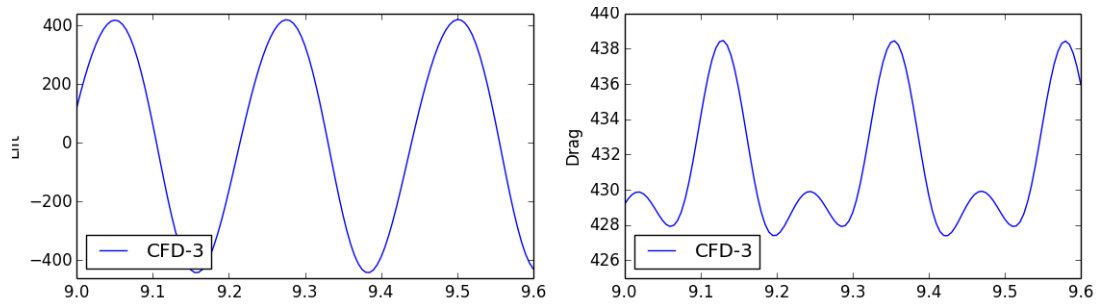
Figure 1.2: CFD-3, flow visualization of velocity time $t = 9s$ Figure 1.3: CFD-3, lift and drag forces at time $t = [9, 9.6]$

Table 1.4: CFD-3

$\Delta t = 0.01 \quad \theta = 0.5$			
nel	ndof	Drag	Lift
1438	6881 (P2-P1)	417.23 +/- 0.0217	-249.21 +/- 0.32
	16474 (P3-P2)	414.86 \pm 5.6282	-7.458 \pm 444.07
2899	13648 (P2-P1)	408.50 \pm 4.3029	-19.731 \pm 373.45
	32853 (P3-P2)	432.86 \pm 5.5025	-9.686 \pm 431.28
7501	34657 (P2-P1)	431.57 \pm 5.2627	-12.497 \pm 429.76
	83955 (P3-P2)	438.20 \pm 5.5994	-11.595 \pm 438.00
19365	88520 (P2-P1)	435.43 \pm 5.4133	-11.545 \pm 438.89
	215219 (P3-P2)	438.80 \pm 5.6290	-11.158 \pm 439.23
Reference		439.95 \pm 5.6183	-11.893 \pm 437.81
Error		0.002 % \pm 0.001 %	0.061 % \pm 0.003%
$\Delta t = 0.005 \quad \theta = 0.5$			
nel	ndof	Drag	Lift
1438	6881 (P2-P1)	417.24 \pm 0.0084	-249.386 \pm 0.1345
1438	16474 (P3-P2)	414.90 \pm 5.7319	-8.467 \pm 443.45
1438	13648 (P2-P1)	408.27 \pm 4.0192	-18.981 \pm 363.84
2899	32853 (P3-P2)	432.90 \pm 5.5333	-11.382 \pm 430.60
1438	34657 (P2-P1)	431.59 \pm 5.2979	-13.644 \pm 429.68
7501	83955 (P3-P2)	438.23 \pm 5.6393	-12.917 \pm 437.78
1438	88520 (P2-P1)	435.46 \pm 5.4579	-13.190 \pm 438.05
19365	215219 (P3-P2)	438.84 \pm 5.6576	-12.786 \pm 438.36
Reference		439.95 \pm 5.6183	-11.893 \pm 437.81
Error		0.002 % \pm 0.006 %	0.075 % \pm 0.001%

1.2.2 Discussion of results

The numerical results for CFD1, CFD2 and CFD3 are all within reasonable range of the reference solutions presented in [1]. For CFD1 and CFD2, the choice of P2-P1 elements together with a fully implicit scheme $\theta = 1$ gained sufficient accuracy in comparison with the reference solution. The second order cranc-nicholoson scheme $\theta = 0.5$ was investigated for CFD1 and CFD2, however only improving the results of order 10^{-6} for both lift and drag. For the periodic problem CFD-3, the choice of P2-P1 elements with a fully implicit time-stepping scheme proved unsuffcient for capturing the expected periodic solution. Only a steady-state flow profile was observed.. By cranc-nicolson time-stepping scheme $\theta = 0.5$, the periodic solution was attained. Since the choice of finite-elemt pair is not reported in the original work, both P3-P2 and P2-P1 element pairs for fluid and pressure repsectivly was compared in combination with spatial mesh refinement. From Table 1.4, the choice P3-P2 element pair is eminent to achieve reasonable results for the first and second

mesh regardless of timestep. However, the third and fourth mesh shows close resemblance with the reference solution.

On this basis, the choice of P2-P1 element pair is sufficient for the evaluation of drag and lift on the inner geometry with increasing mesh resolution.

1.2.3 Validation of solid solver

The first validation

1.2.4 Validation of fluid structure interaction solver

The validation of the FSI solver consist of three sub-cases which will be referred to FSI-1, FSI-2 and FSI-3. The FSI-1 environment yields a steady state solution for the system, inducing small deformations to the elastic flag. This environment is exelent to ensure the overall coupling of the FSI-problem is exectuted properly. The FSI-2 and FSI-3 environment results in a periodic solution, where the elastic flag oscilates behind the cylinder.

For all sub-cases a parabolic velocity profile on the form,

$$v_f(0, y) = 1.5U \frac{(H - y)y}{(\frac{H}{2})^2}$$

is set on the left channel inflow. H is the height of the channel, while the parameter U is set differently to each problem to induce different flow profiles. At the right channel outflow, the pressure is set to $p = 0$. No-slip boundary conditions for the fluid are enforced on the channel walls, and on the circle of the inner geometry. The structure deformation and velocity is set to zero on the left side of the flag, where the flag is ancored to the circle. On the fluid-structure interface Γ , we enforce the kinematic and dynamic boundary condition

$$\mathbf{v}_f = \mathbf{v}_s \quad (1.1)$$

$$\sigma_f \cdot \mathbf{n} = \sigma_s \cdot \mathbf{n} \quad (1.2)$$

From chapter ?, (1.1) is enforced strongly due to the continious velocity field, while (1.2) is enforced weakly by omtitting form the weak formulation by.

Apart from the accuracy of the reported values, the main purpose of the validation of the fluid solver is twofold. Firstly, it is of great importance to ensure that the overall coupling of the fluid-structure interaction problem are executed correctly. Second, a good choice of mesh extrapolation model is essential to ensure that mesh entanglement is not present.

Table 1.5: Benchmark environment

Solid parameters			
parameter	FSI1	FSI2	FSI3
$\rho^s [10^3 \frac{kg}{m^3}]$	1	10	1
ν^s	0.4	0.4	0.4
$\mu^s [10^6 \frac{kg}{ms^2}]$	0.5	0.5	2.0
Fluid parameters			
$\rho^f [10^3 \frac{kg}{m^3}]$	1	1	1
$\nu^f [10^{-3} \frac{m^2}{s}]$	1	1	1
U	0.2	1	2
parameter	FSI1	FSI2	FSI3
Re	20	100	200

FSI1

Table 1.6: FSI 1 Results

Laplace					
nel	ndof	ux of A [x 10 ³]	uy of A [x 10 ³]	Drag	Lift
2474	21249	0.0226	0.8200	14.061	0.7542
7307	63365	0.0227	0.7760	14.111	0.7517
11556	99810	0.0226	0.8220	14.201	0.7609
Reference		0.0227	0.8209	14.295	0.7638
Linear Elastic					
nel	ndof	ux of A [x 10 ³]	uy of A [x 10 ³]	Drag	Lift
2474	21249	0.0226	0.8198	14.061	0.7541
7307	63365	0.0227	0.7762	14.111	0.751
11556	99810	0.0226	0.8222	14.201	0.7609
Reference		0.0227	0.8209	14.295	0.7638
Biharmonic bc1					
nel	ndof	ux of A [x 10 ³]	uy of A [x 10 ³]	Drag	Lift
2474	21249	0.0226	0.8200	14.061	0.7541
7307	63365	0.0227	0.7761	14.111	0.7517
11556	99810	0.0227	0.8017	14.205	0.9248
Reference		0.0227	0.8209	14.295	0.7638
Biharmonic bc2					
nel	ndof	ux of A [x 10 ³]	uy of A [x 10 ³]	Drag	Lift
2474	21249	0.0226	0.8200	14.061	0.7543
7307	63365	0.0227	0.7761	14.111	0.7518
11556	99810	0.0227	0.8020	14.205	0.9249
Reference		0.0227	0.8209	14.295	0.7638

Table 1.7: FSI 1 - No extrapolation

No extrapolation					
nel	ndof	ux of A [x 10 ³]	uy of A [x 10 ³]	Drag	Lift
2474	21249	0.0224	0.9008	14.064	0.7713
7307	63365	0.0226	0.8221	14.117	0.7660
11556	99810	0.0225	0.8787	14.212	0.7837
REF	REF	0.0227	0.8209	14.295	0.7638

FSI2

FSI2

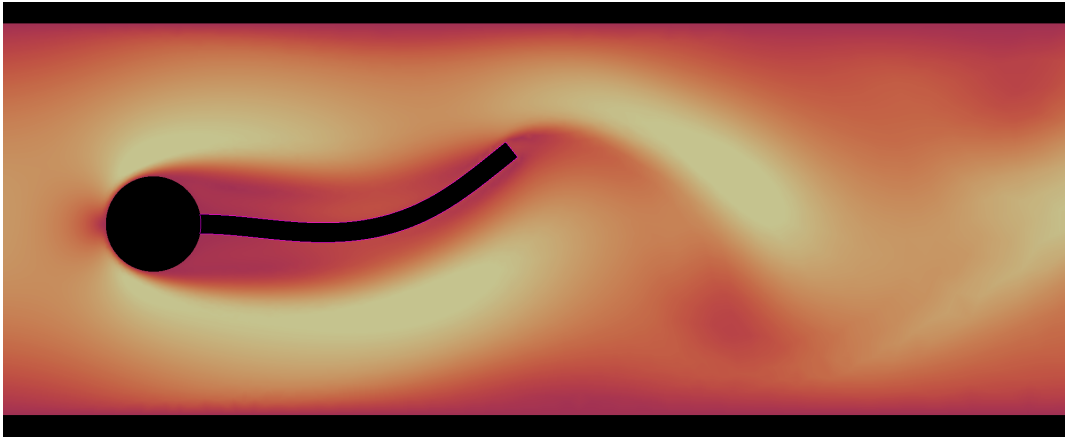


Figure 1.4: FSI-2, visualization of fully developed flow with structure deformation at time $t = 9s$

FSI3

Table 1.8: FSI 3 - Comparison of mesh extrapolation models

Laplace $\Delta t = 0.01\theta = 0.51$					
nel	ndof	ux of A [x 10 ³]	uy of A [x 10 ³]	Drag	Lift
2474	21249	-2.41 \pm 2.41	1.49 \pm 3.22	449.40 \pm 14.70	0.55 \pm 155.80
7307	63365	-2.32 \pm 2.30	1.34 \pm 3.17	451.78 \pm 16.08	1.13 \pm 151.22
11556	99810	-2.34 \pm 2.34	1.57 \pm 3.19	455.92 \pm 17.32	-0.10 \pm 151.03
$\Delta t = 0.001\theta = 0.501$					
nel	ndof	ux of A [x 10 ³]	uy of A [x 10 ³]	Drag	Lift
1216	5797	-2.17 \pm 2.08	3.32 \pm 29.07	439.98 \pm 14.08	1.91 \pm 151.71
2295	10730	-3.04 \pm 2.88	1.51 \pm 35.88	452.04 \pm 22.41	3.30 \pm 160.11
5963	27486	-3.03 \pm 2.85	1.23 \pm 35.97	459.45 \pm 23.80	1.53 \pm 160.14
Reference		136.7	10.53		
Error		0.007 %	0.001 %		

Biharmonic 1 $\Delta t = 0.01\theta = 0.51$					
nel	ndof	ux of A [x 10 ³]	uy of A [x 10 ³]	Drag	Lift
2474	21249	7.96 \pm 8.10	-3.84 \pm 1.02	450.16 \pm 15.11	-20.09 \pm 148.17
7307	63365	3.10 \pm 3.06	-1.90 \pm 4.21	457.37 \pm 15.24	-51.77 \pm 127.28
11556	99810	-2.18 \pm 9.65	1.31 \pm 4.93	456.40 \pm 17.45	0.45 \pm 149.68
$\Delta t = 0.001\theta = 0.5$					
nel	ndof	ux of A [x 10 ³]	uy of A [x 10 ³]	Drag	Lift
1216	5797	-2.18 \pm 2.10	3.56 \pm 2.90	435.19 \pm 9.77	-1.57 \pm 151.43
7307	63365	-1.42 \pm 4.70	7.77 \pm 2.85	454.38 \pm 19.75	17.97 \pm 155.08
11556	99810	-2.23 \pm 6.16	1.72 \pm 4.48	459.12 \pm 22.97	-3.12 \pm 171.22
Reference		-2.69 \pm 2.56	1.48 \pm 34.38	457.3 \pm 22.66	2.22 \pm 149.78
Error		0.007 %	0.001 %		

Biharmonic 2 $\Delta t = 0.01\theta = 0.51$					
nel	ndof	ux of A [x 10 ³]	uy of A [x 10 ³]	Drag	Lift
1216	5797	-1.74 \pm 1.76	3.56 \pm 26.01	439.41 \pm 12.21	-1.35 \pm 138.74
2295	10730	-2.39 \pm 2.40	1.76 \pm 32.27	449.71 \pm 18.16	3.71 \pm 149.97
$\Delta t = 0.001\theta = 0.501$					
nel	ndof	ux of A [x 10 ³]	uy of A [x 10 ³]	Drag	Lift
1216	5797	-3.39 \pm 3.38	1.23 \pm 36.61	413.26 \pm 51.82	57.19 \pm 222.65
2295	10730	-4.70 \pm 4.71	1.49 \pm 44.62	427.91 \pm 93.17	44.38 \pm 268.05
Reference		-2.69 \pm 2.56	1.48 \pm 34.38	457.3 \pm 22.66	2.22 \pm 149.78
Error		0.007 %	0.001 %		

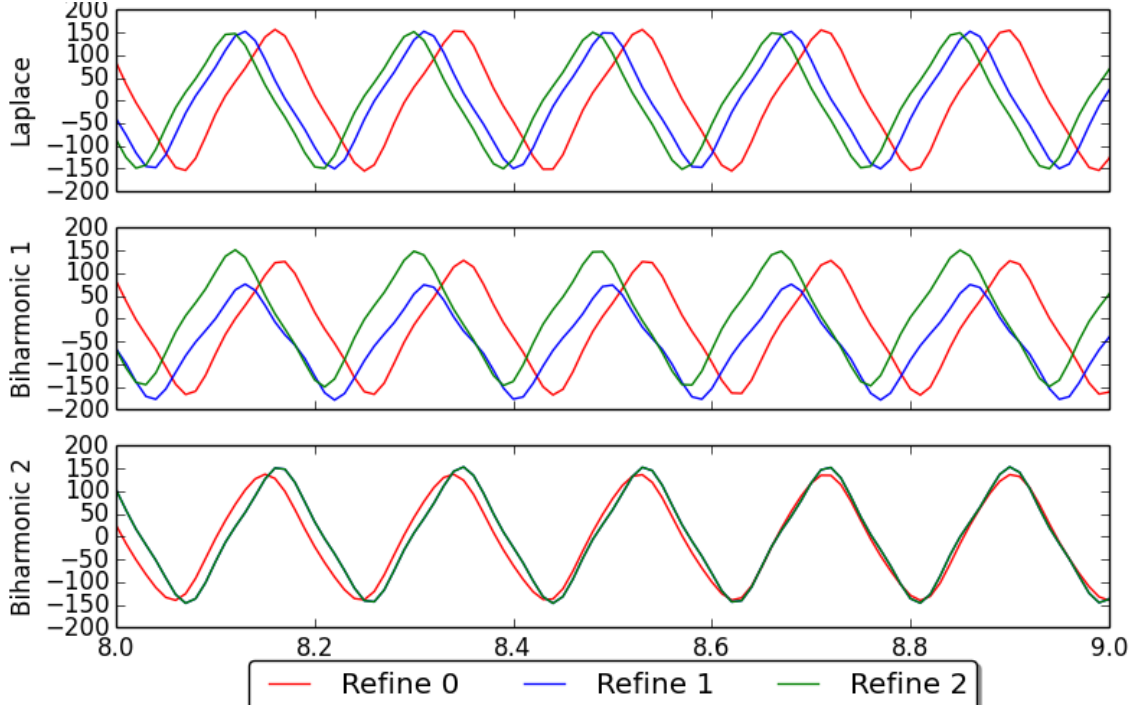


Figure 1.5: Comparing mesh extrapolation models

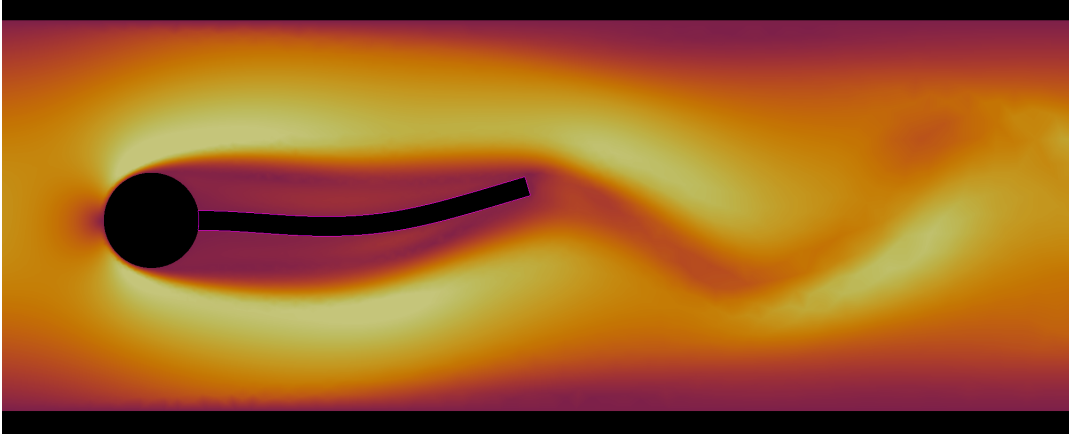


Figure 1.6: FSI-3, visualization of fully developed flow with structure deformation at time $t = 5.1s$

1.2.5 Discussion of results

Considering FSI1, all mesh extrapolation models are of high accuracy compared to the reference solution. However, due to the small deformations of order 10^{-6} , FSI1 doesn't provide a rigorous test of the chosen mesh extrapolation model. By omitting mesh extrapolation from the variational formulation, reasonable results are still obtained. This proves that the FSI-1 validation case can be misleading, in terms of validating the chosen mesh extrapolation model.

The FSI2 case proved to be one of the most demanding tests, due to the large deformation of the elastic flag. leading to the risk of entangled mesh cells. Therefore

a high quality extrapolation of the solid deformation into the fluid is needed. All mesh extrapolation models proved to be unstable. The FSI3 environment does not induce deformation to the extent of the FSI2. However a critical phase in the transition to the periodic solution was discovered, where the pressure oscillation induces a large deformation to the system.

1.2.6 Investigation of temporal stability

It is known that the Crank-Nicolson scheme can suffer from temporal stability, for long-term simulations [?].

Preliminary work regarding discretization and numerical analysis of Crank-Nicholson time stepping schemes for fluid structure interaction can be found in cite Wick papers. Two main properties of interest of higher-order methods have proven to be the stability of long-time simulation, and obtaining the expected physics for the problem of interest.

The authors of [?], investigated temporal stability of the Crank-Nicolson scheme for the validation benchmark found in [1]. The criteria for the numerical experiments was to obtain a stable solution in the time interval $[0, 10]$ minutes, by temporal and spatial refinement studies. The fully monolithic FSI problem discretized with second-order Crank-Nicolson, proved to give general stability problems for long-term simulation.

Following the ideas of [?], a second order scheme based on the Crank-Nicolson yields two possibilities.

Discretization 1.1. *Crank-Nicolson secant method*

$$\left[\frac{\hat{\mathbf{J}}(\hat{\mathbf{u}}^n) \hat{\nabla} \hat{\mathbf{v}}^n \hat{\mathbf{F}}_W^{-1}}{2} + \frac{\hat{\mathbf{J}}(\hat{\mathbf{u}}^{n-1}) \hat{\nabla} \hat{\mathbf{v}}^{n-1} \hat{\mathbf{F}}_W^{-1}}{2} \right] \frac{\hat{\mathbf{u}}^n - \hat{\mathbf{u}}^{n-1}}{k}$$

Discretization 1.2. *Crank-Nicolson midpoint-tangent method*

$$\left[\frac{\hat{\mathbf{J}}(\hat{\mathbf{u}}_{cn}) \hat{\nabla} \hat{\mathbf{v}}_{cn} \hat{\mathbf{F}}_W^{-1}}{2} \right] \frac{\hat{\mathbf{u}}^n - \hat{\mathbf{u}}^{n-1}}{k} \quad \hat{\mathbf{u}}_{cn} = \frac{\hat{\mathbf{u}}^n + \hat{\mathbf{u}}^{n-1}}{2} \quad \hat{\mathbf{v}}_{cn} = \frac{\hat{\mathbf{v}}^n + \hat{\mathbf{v}}^{n-1}}{2}$$

The numerical experiments showed very similar performance for Discretization 1.1 and 1.2, and significant differences of temporal accuracy was not found.

Two options to cope with the presented instabilities are the *shifted Crank-Nicolson* [?], [?], [?], and the *frac-step method*. Both of these methods are defined as A-stable time-stepping schemes meaning.. In this thesis the shifted Crank-Nicolson scheme will be considered.

The shifted Crank-Nicolson scheme introduce further stability to the overall system, by shifting the θ parameter slightly to the implicit side. If the shift is dependent of the time-step k such that $\theta \leq \frac{1}{2} + k$, the scheme will be of second order [?].

1.3 Optimization of Newtonsolver

The expression *bottleneck* express a phenomen where the total performance of a complete implementation is limited to small code fragments, accounting for the primary consumption of computer resources.

As for many other applications, within computational science one can often assume the consummation of resources follows the *The Pareto principle*. Meaning that for different types of events, roughly 80% of the effects come from 20% of the causes. An analogy to computational sciences it that 80% of the computational demanding operations comes from 20% of the code. In our case, the bottleneck is the newtonsolver. The two main reasons for this is

- **Jacobian assembly**

The construction of the Jacobian matrix for the total residue of the system, is the most time demanding operations within the whole computation.

- **Solver.**

As iterative solvers are limited for the solving of fluid-structure interaction problems, direct solvers was implemented for this thesis. As such, the operation of solving a linear problem at each iteration is computational demanding, leading to less computational efficient operations. Mention order of iterations?

Facing these problems, several attempts was made to speed-up the implementation. The FEniCS project consist of several nonlinear solver backends, were fully user-customization option are available. However one main problem which we met was the fact that FEniCS assembles the matrix of the different variables over the whole mesh, even though the variable is only defined in one to the sub-domains of the system. In our case the pressure is only defined within the fluid domain, and therefore the matrix for the total residual consisted of several zero columns within the structure region. FEniCS provides a solution for such problems, but therefore we were forced to construct our own solver and not make use of the built-in nonlinear solvers.

The main effort of speed-up were explored around the Jacobian assembly. Of the speed-ups methods explored in this thesis, some are *consistent* while others are *nonconsistent*. Consistent methods are methods that always will work, involving smarter approaches regarding the linear system to be solved. The non-consistent method presented involves altering the equation to be solved by some simplification of the system. As these simplifications will alter the expected convergence of the solver, one must take account for additional Newton iterations against cheaper Jacobi assembly. Therefore one also risk breakdown of the solver as the Newton iterations may not converge.

1.4 Consistent methods

1.4.1 Jacobi buffering

By inspection of the Jacobi matrix, some terms of the total residue is linear terms, and remain constant within each time step. By assembling these terms only in the

first Newton iteration will save some assembly time for the additional iterations needed each time step. As consequence the convergence of the Newton method should be unaffected as we do not alter the system.

1.5 Non-consistent methods

1.5.1 Reuse of Jacobian

As the assembly of the Jacobian at each iteration is costly, one approach of reusing the Jacobian for the linear system was proposed. In other words, the LU-factorization of the system is reused until the Jacobi is re-assembled. This method greatly reduced the computational time for each time step. By a user defined parameter, the number of iterations before a new assembly of the Jacobian matrix can be controlled.

1.5.2 Quadrature reduce

The assemble time of the Jacobian greatly depends on the degree of polynomials used in the discretisation of the total residual. Within FEniCS this parameter can be controlled, and as such we can specify the order of polynomials representing the Jacobian. The use of lower order polynomials reduces assemble time of the matrix at each newton-iteration, however it leads to an inexact Jacobian which may results to additional iterations.

Table 1.9: Comparison of speedup techniques

Implementation	Naive	Reducequad.	Reusejacobi	Combined
Mean time/- timestep	104.5	125.5	48.3	6.8
Speedup	1.0	1.20	0.46	0.06
Mean iteration	4.49	30.59	10.29	10.29

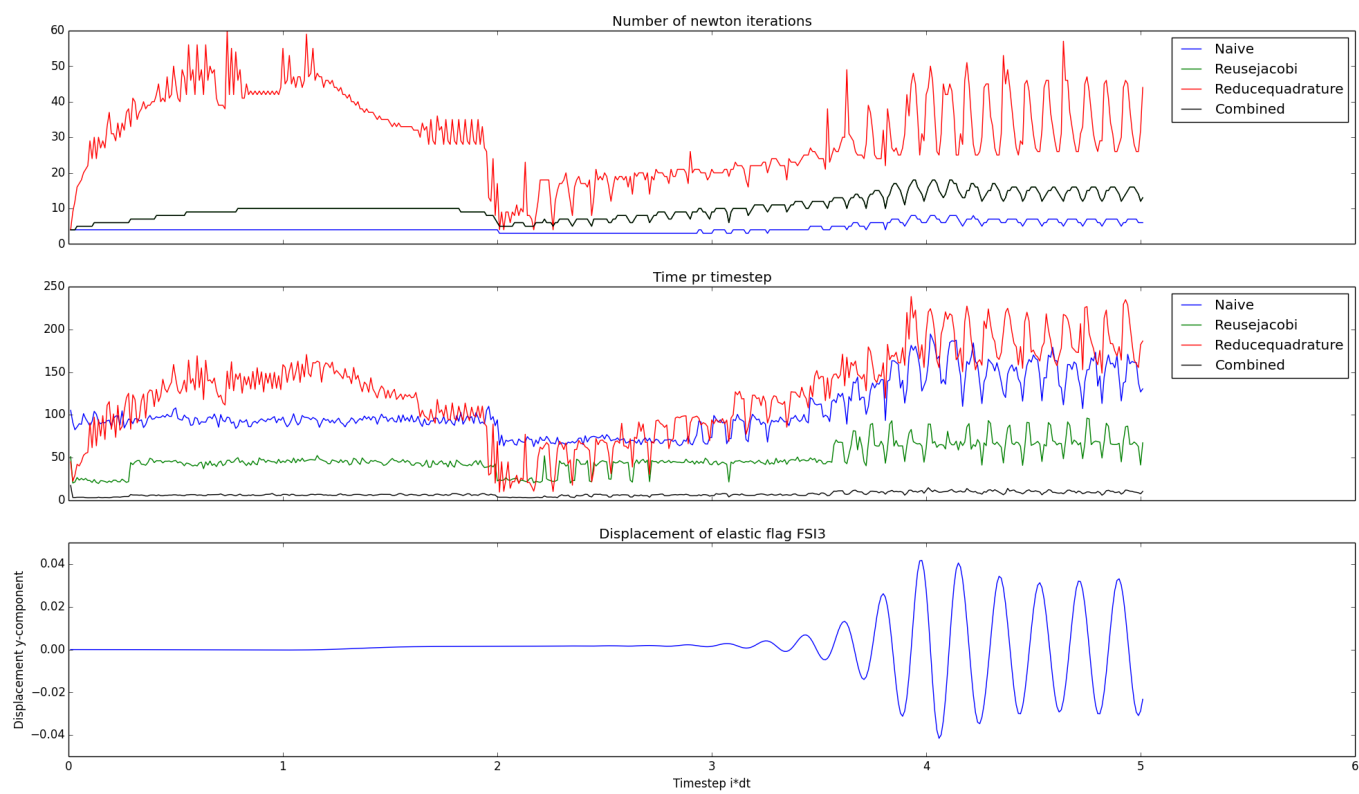


Figure 1.7: Computational domain of the validation benchmark

Bibliography

- [1] Jaroslav Hron and Stefan Turek. Proposal for numerical benchmarking of fluid-structure interaction between an elastic object and laminar incompressible flow. *Fluid-Structure Interaction*, 53:371–385, 2006.